Review Article

First-Arrival Picking for Microseismic Monitoring Based on Deep Learning

Xiaolong Guo [1,2]

[1]*School of Electronic and Information, Yangtze University, Jingzhou 434023, China*
[2]*National Demonstration Center for Experimental Electrical & Electronical Education, Yangtze University, China*

Correspondence should be addressed to Xiaolong Guo; 201800911@yangtzeu.edu.cn

In microseismic monitoring, achieving an accurate and efficient first-arrival picking is crucial for improving the accuracy and efficiency of microseismic time-difference source location. In the era of big data, the traditional first-arrival picking method cannot meet the real-time processing requirements of microseismic monitoring process. Using the advanced idea of deep learning-based end-to-end classification and the prominent feature extraction advantages of a fully convolution neural network, this paper proposes a first-arrival picking method of effective signals for microseismic monitoring based on UNet++ network, which can significantly improve the accuracy and efficiency of first-arrival picking. In this paper, we first introduced the methodology of the UNet++-based picking method. And then, the performance of the proposed method is verified by the experiments with finite-difference forward modeling simulated signals and actual microseismic records under different signal-to-noise ratios, and finally, comparative experiments are performed using the U-Net-based first-arrival picking algorithm and the Short-Term Average to Long-Term Average (STA/LTA) algorithm. The results show that compared to the U-Net network, the proposed method can obviously improve the first-arrival picking accuracy of the low signal-to-noise ratio microseismic signals, achieving significantly higher accuracy and efficiency than the STA/LTA algorithm, which is famous for its high efficiency in traditional algorithms.

1. Introduction

The processing of microseismic monitoring data has confronted with difficulty in balancing accuracy and efficiency for a long time [1–3]. With the development of microseismic monitoring technology, hydraulic fracturing microseismic has become increasingly important in shale gas exploration and development [4–7]. Accurate and efficient first-arrival picking of microseismic monitoring is the premise for improving the performance of microseismic time-difference source location. Recently, many picking methods have been proposed, such as the Short-Term Average to Long-Term Average (STA/LTA) [8], Akaike information criterion (AIC) [9], and correlation method [10].

Recently, certain progress in the research of first-arrival picking has been achieved. Sheng [11] combined the wavelet transform with the high-order statistics and used the high-order statistics to pick the first arrival of signals after con-ducting the wavelet multiscale analysis, which suppressed random noise to a certain extent and enhance the accuracy of first-arrival picking. Shimoda [12] employed the cross-correlation method to identify the first arrival of the microseismic signal in the borehole common geophone gathers, thus providing simpler picking of the first-arrival time and higher accuracy than previous step-by-step arrival picking methods using a single detector. On the basis of previous studies, Tan et al. [13] proposed a first-arrival picking method of microseismic signals under low signal-to-noise ratio (SNR). Firstly, the cross-correlation and the least squares criterion were used to preprocess the original microseismic data to obtain a better time difference correction, and then, the multichannel semblance parameter was used to identify the microseismic events. After the microseismic events had been identified, the arrivals of records were picked. Karastathis [14] used time-frequency analysis to obtain a picking method of the first arrival of microseism,

and compared with the traditional method, the picking accuracy was improved significantly. Massin [15] used the component energy correlation method to identify microseismic body waves. Further, after analyzing the energy ratio algorithm, the high-order statistics method, and the minimum information criterion (AIC) method, Akram et al. [16] found that different methods had their own advantages and disadvantages under different conditions, so they designed a set of parameter-optimized first-arrival picking methods for microseismic signals, namely, different parameters were assigned to different first-arrival picking methods according to the microseismic signal conditions. Dowan et al. [17] proposed a first-arrival picking method of noisy microseismic records by combining the cross-correlation and superposition process. The results showed that this method could automatically pick the first arrival for low-SNR signals. Yu et al. [18] proposed a first-arrival picking method based on the multichannel waveform cross-correlation. The results showed that the first arrival consistency of the proposed method is improved compared with the traditional single-track picking method. Raj et al. [19] proposed a first-arrival picking method of microseisms based on the two-dimensional constant false alarm rate, which improved the first-arrival picking accuracy under the low-SNR conditions. Qu et al. [20] used the supervised support vector machine algorithm to pick the first arrival automatically, improving the efficiency of first-arrival picking. Sheng et al. [21] developed the Shearlet Transform-Short time window/Long time window-Kurtosis (S-S/L_K) algorithm using the Shearlet transform and high-order statistics, which could accurately pick the first arrival of low-SNR microseismic signals. Gao et al. [22] used a sliding window combined with the fuzzy C-means clustering algorithm to pick the first arrival of noisy and preprocessed microseismic signals. However, at a large amount of monitoring data, the above traditional first-arrival picking method cannot simultaneously meet the requirements for efficiency and accuracy of real-time microseismic monitoring.

The deep convolutional neural networks have been widely researched because of their outstanding feature extraction and recognition performances [23–26]. Zhang et al. [27] proposed a new multifeature reweighted DenseNet (MFR-DenseNet) architecture for image classification, which greatly reduced the error rate on CIFAR-10 and CIFAR-100 datasets. Han et al. [28] proposed to add the edge convolution constraint to the improved U-Net for target detection to predict the significant mapping of an image. The improved U-Net integrates the characteristics of different layers and thus greatly reducing the information loss. Qu et al. [29] proposed a radar signal intrapulse modulation recognition method, which uses the time-frequency analysis, image processing, and convolutional neural network (CNN) to modulate and recognize the radar signal. At the signal-to-noise ratio of -6 dB, this method achieved the recognition success rate of 96.1%. Yang et al. [30] proposed a detection model based on a multitask rotating region convolutional neural network and achieved good results in arbitrary directional ship position detection and direction prediction.

Recently, in the field of geophysics, researches have also been conducted by many scholars. Xu et al. [31] identified active earthquake events using the convolution neural network. Chen et al. [32] achieved strong noise interference suppression of magnetotelluric data using the recurrent neural network (RNN). It is worth mentioning that Chen, Zhang, and Saad [33–38] have made excellent contributions to the field of geophysics by applying deep learning to microseismic events.

Due to the jump layer connection, deep supervision structure, and the advantages of end-to-end classification and integration of deep and shallow features [39–42], the UNet++ [43] has been widely used in the field of medical image processing [44]. Following the advanced idea of deep learning-based end-to-end classification, this paper considers the first-arrival picking of effective microseismic signals as a two classification problem and uses UNet++ network to pick the first-arrival of effective microseismic signals, improving the fault-tolerant performance and correcting the prediction deviation caused by labeling error using the label smoothing and regularization; finally, it outputs the maximum probability prediction value corresponding to the first-arrival category as the first arrival point.

The rest of the paper is organized as follows. I introduce the methodology of the first-arrival picking method based on UNet++. And then, data sets are constructed, and the UNet++ is optimized to obtain the best hyperparameter. The first arrivals are determined by the UNet++, and comparative experiments are conducted using the U-Net-based first-arrival picking algorithm and the STA/LTA algorithm according to the finite difference forward modeling simulated signals and actual microseismic records at different signal-to-noise ratios. The results show that compared with the U-Net network, the proposed method can obviously improve the first-arrival picking accuracy of the low-SNR microseismic signals, achieving significantly higher accuracy and efficiency than the STA/LTA algorithm, which is well-known for its high efficiency in traditional algorithms. Finally, the discussion and solution are presented, respectively.

2. Methods

2.1. UNet++-Based Picking Method. U-Net is an advanced and mature network, which combines the special structure of up-sampling and down-sampling to play an important role in the field of deep learning. Compared to the U-Net network, the UNet++ network, which is presented in Figure 1, has a deeper receptive field. UNet++ owns a skip connection structure and deep supervision based on the structure of U-Net, which can handle higher-dimensional information. The main advantages of the UNet++ are as follows: its unique skip connection integrates the characteristics of different layers, which improves accuracy; it has a deep supervision framework, that is $L_i (i = 1, 2, 3, 4)$, so it gets the final output result by averaging four split branches and which reduces the number of parameters and improves the speed and accuracy of the network. The workflow of the UNet++-based picking method is as follows:
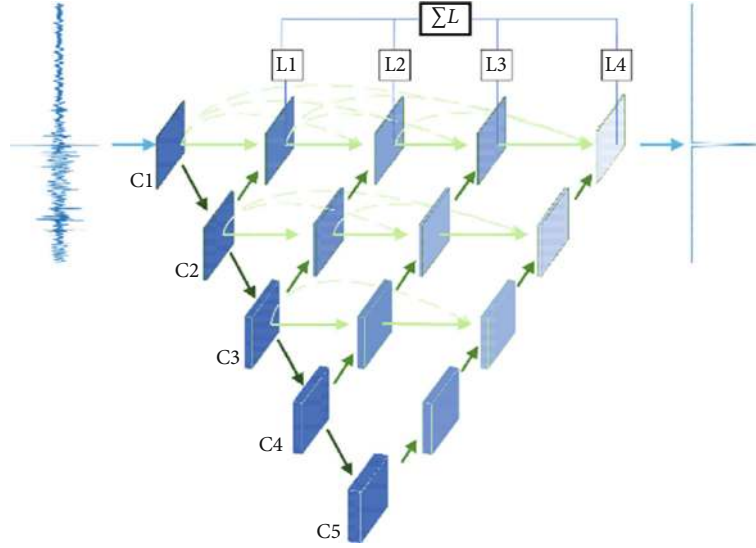
FIGURE 1: UNet++ model structure.

(1) Input: Discrete time series of microseismic signal.

(2) Contraction Path of UNet++: The main function of this path is to extract the signal and noise features of microseismic signals. Each layer of the contraction path contains a convolution layer, an activation function layer, a batch normalization layer, and a maximum pooling layer; all layers except the first large layer contain an up-sampling layer. The convolution kernel in the convolutional layer has a size of 3×3; the size of the convolution kernel in the up-sampling layer is 2×2; the activation function used in the activation function layer is Leaky Relu, which is expressed as:

$$f(x_i) = \begin{cases} x_i, & x_i \geq 0, \\ ax_i, & x_i < 0, \end{cases} \quad (1)$$

where a represents a trainable learning parameter, and in this work, it is set to 0.01; x_i denotes the network input; $f(x_i)$ represents the output. The Leaky Relu function can solve the problem of gradient disappearance caused by layer depth and accelerate the convergence speed.

(3) The Expansion Path of UNet++: The expansion path uses up-sampling to restore and decode the features to the original input size and recover the spatial resolution of the input signal, restore the detailed features, and achieve the end-to-end classification effect.

(4) Output: In order to make the extracted features more comprehensive, the average value of the branches obtained by the pruning operation is used to obtain the output result. Before the training, the one-hot encoding of the labels is used to obtain the sparse labels, and then, the label smoothing and regularization processing given by (2) are used to improve pre-

diction accuracy of the model and increase its ability to resist label error. Finally, the softmax function given by (3) is used to obtain the probability curve of the signal sampling point belonging to the first-arrival category, and the point with the maximum probability on the curve is taken as the first-arrival point. The softmax cross-entropy is used as the network loss function to optimize the network model, and it is given by (4).

$$y' = (1 - \varepsilon) * y + \varepsilon * \mu. \quad (2)$$

In (2), y' denotes the sample label after label smoothing, ε represents the smoothing factor, y represents the original sample, and μ is an introduced fixed distribution of all values of 1.

$$F_i'(x) = \frac{e^{g_i(x)}}{\sum_{k=1}^{n} e^{g_k(x)}}, \quad (3)$$

$$L\left(f_i'(x), F_i'(x)\right) = -\sum_{i=1}^{n} \sum_{x} \left(f_i'(x) \log F_i'(x)\right). \quad (4)$$

In (3) and (4), i signifies types, x denotes the sampling point, $g_i(x)$ denotes the output of the last layer of the UNet++ network corresponding to sampling point x, $f_i'(x)$ indicates the probability distribution of real labels, and $F_i'(x)$ represents the network prediction probability distribution. Figure 2 shows the flow of the paper. Figure 3 shows the process of labeling the first arrival.

2.2. Experiment. The parameters of the experimental platform are given in Table 1.

2.3. Dataset. The quality and richness of a dataset have a significant influence on the picking ability of the UNet++.
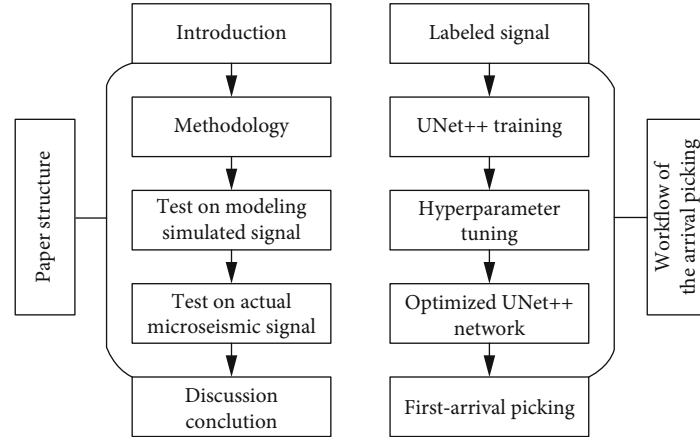
Figure 2: The structure and technical route of the paper.
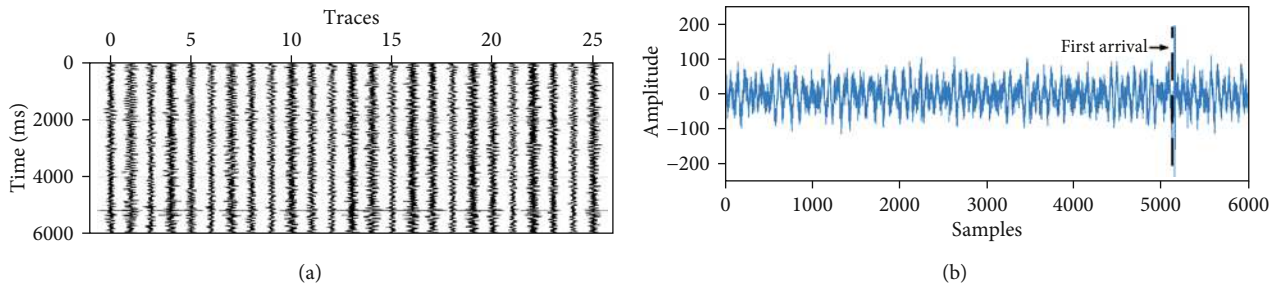

Figure 3: Labeling the first arrival. (a) Microseismic signal profile. (b) The fifth signal in the profile.

Table 1: Experimental platform parameters.

	CPU	IntelCorei7-9750H
Hardware environment	GPU	GeForceGTX1660 Ti
	RAM	20GB
		Ubuntu 16.04
Software environment	Platform	Tensorflow1.12
		CUDA9.0+Cudnn7.1
		Pycharm+Python3.6

Therefore, when constructing the training set of the UNet++, it is necessary to consider the relationship between the trace continuity and the changing trends of the model parameters with the distance between the breaking and receiving points of the signal at the arrival point. In this paper, the dataset consisted of 5000 simulated signals produced by the forward modeling and 5000 real microseismic monitoring signals collected from Hubei, Sichuan, and Shengli Oilfield in China with high and low SNR. The simulated signals were in the frequency range of 20–1000 Hz and was generated by the finite difference forward modeling at different SNR values using different velocity models. The data was divided into the training set, test, and validation sets using the ratio of 6 : 2 : 2. Finally, automatic picking method, the Shearlet Transform-Short time window/Long time window-Kurtosis (S-S/L-K) method [43], and manual picking method were used to label the arrival points in the training set.

2.4. Hyperparameter Optimization.
The learning rate and label smoothing regularization factor were optimized to determine the most suitable hyperparameters of the UNet++. The learning rate, as one of the most important hyperparameters that affect the network model performance, directly determines the convergence speed and training accuracy of the network. The smoothing regularization factor can affect the intensity of disturbance applied to correct labels, thus affecting the correctness of network input labels. Therefore, before using the UNet++ to pick the first arrival, it is necessary to optimize the most important hyperparameters to maximize model performance.

(1) Learning Rate Optimization: As already mentioned, as one of the most important hyperparameters, the learning rate directly affects the prediction performance of the network. On the one hand, if the learning rate is too large, the network will miss the extreme value point, which will reduce the network training accuracy. On the other hand, if the learning rate is too low, the network will converge too slowly or even the overfitting problem can be caused. In order to solve this issue, in this work, the optimal learning rate was determined by evaluating the model's performances at the learning rate of 0.01, 0.001, and 0.0001. The model loss and accuracy on the training and validation sets at different learning rates are presented in Figures 4(a) and 4(b), respectively. As presented in Figures 4(a) and 4(b), at the learning rate
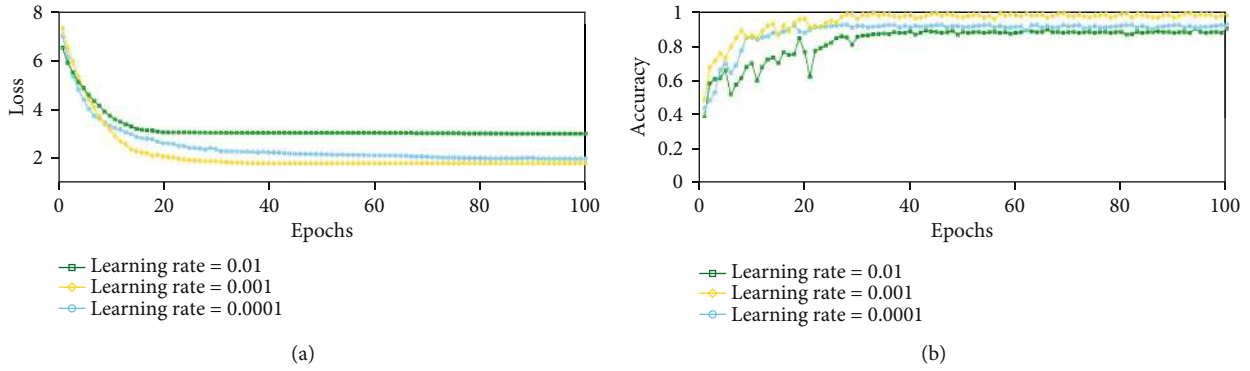
(a)

(b)

Figure 4: Training and validation curves at different initial learning rates. (a) Model loss on the training set. (b) Model accuracy on the validation set.
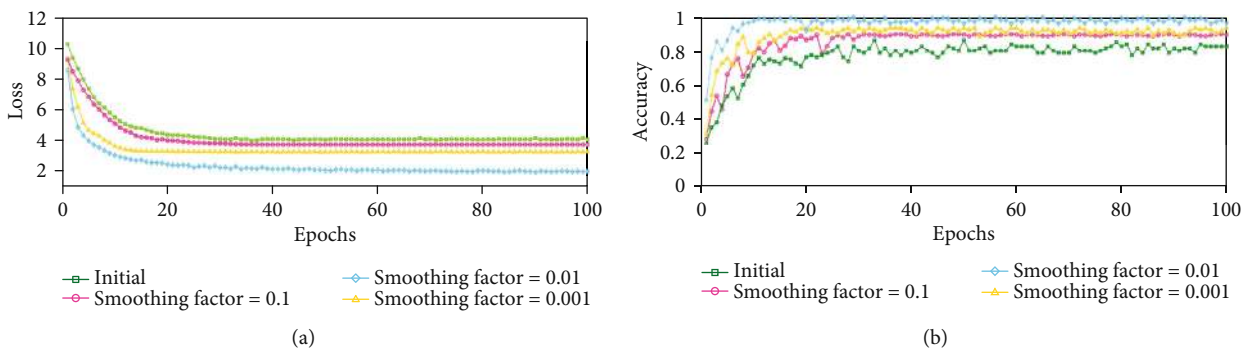

(a)

(b)

Figure 5: Training and validation curve before and after label smoothing. (a) Model loss on the training set. (b) Model accuracy on the validation set.
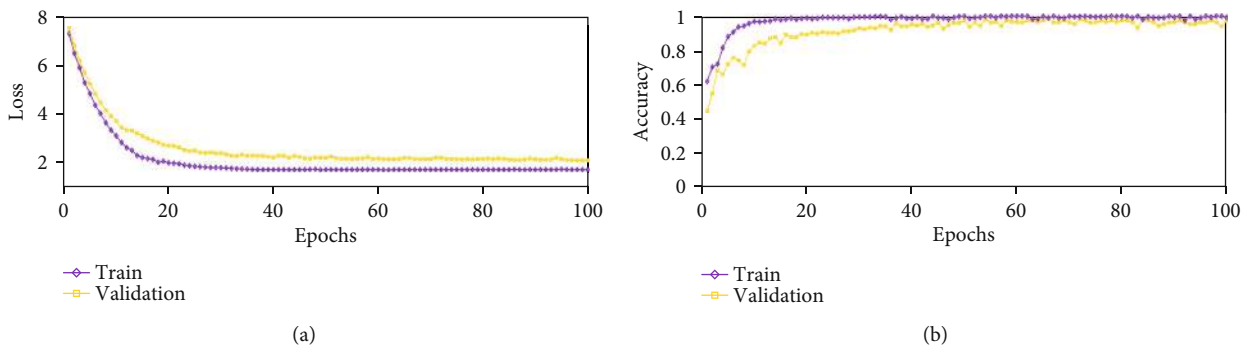

(a)

(b)

Figure 6: Comparison of model performance on the training and validation sets. (a) Loss comparison. (b) Accuracy comparison.

of 0.001, the model converged faster and obtained the highest validation accuracy. Therefore, the learning rate of 0.001 was used as the initial learning rate in the experiments.

(2) Label Smoothing: Label smoothing regularization enhances the model's ability to tolerate input label error by adding disturbances to the original label. The label smooth regularization factor can determine the strength of the applied disturbance. On the one hand, if the regularization factor is too large, the network can difficultly converge because the label perturbation will be too strong. On the other hand,
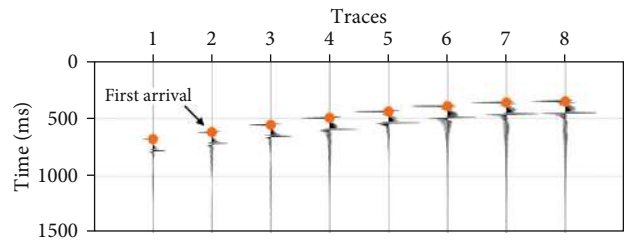

Figure 7: Forward modeling simulated signal profile.

if the regularization factor is too small, it will lead to a decrease in network fault tolerance. Therefore, it is very important to choose an appropriate
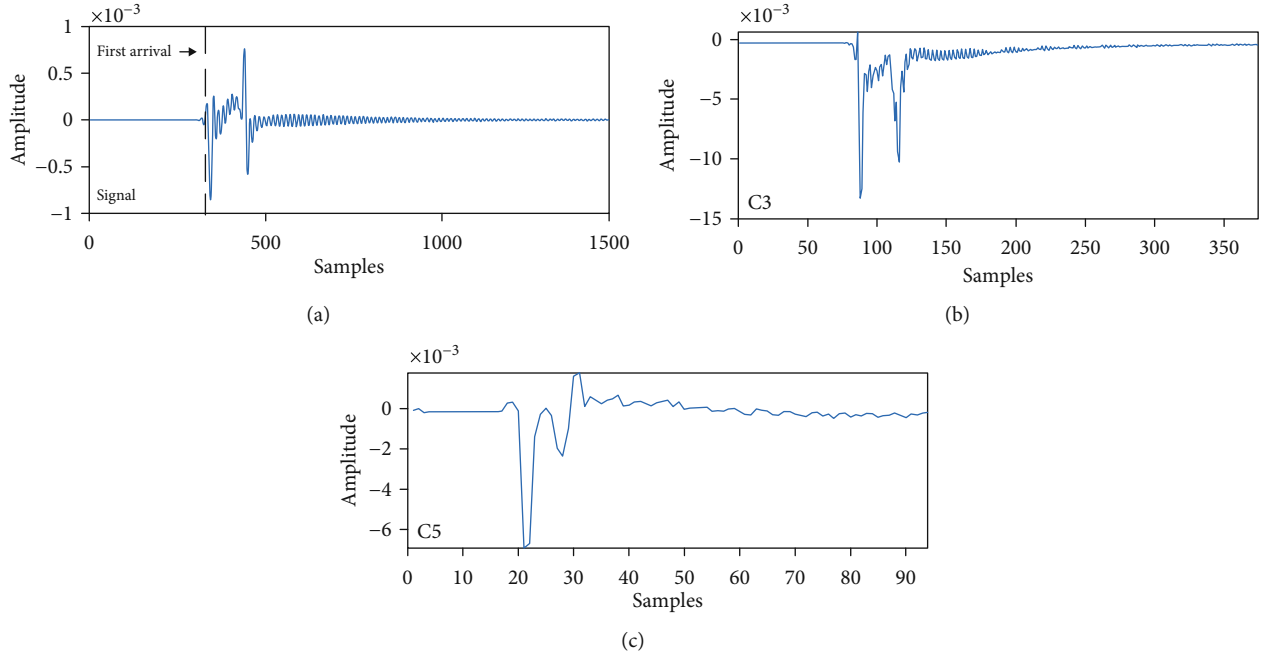
(a)

(b)

(c)

FIGURE 8: Noise-free forward modeling signal and its intermediate features extracted by the UNet++. (a) The noise-free forward modeling signal. (b) Intermediate features of the signal extracted by C3 layer. (c) Intermediate features of the signal extracted by C5 layer.

regularization factor. The loss curve during the training phase and the accuracy curve during the verification phase at different labels smoothing regularization factor values are presented in Figures 5(a) and 5(b), respectively. As presented in Figures 5(a) and 5(b), after the label smoothing is used, the training loss and verification accuracy of the network were significantly improved. Particularly, at the regularization factor of 0.01, the model achieved the best performance. Therefore, the regularization factor of 0.01 was used in the experiments.

(3) Model Validation: In order to verify the generalization ability of the network, the performance of the UNet++ on the training and verification sets was compared, and the fivefold cross-validation was used to evaluate the true generalization error of the network. The loss and accuracy of the UNet++ during the training and validation are presented in Figure 6. According to the results shown in Figures 6(a) and 6(b), the optimized model can be used to pick the first arrival of the microseismic signal accurately.

2.5. Synthetic Examples. The finite-difference forward modeling signal profile, at the signal frequency of 20 Hz, the model size of 301×160, the spatial sampling interval dx = dz = 10, the source coordinate (140.80), and the two-layer velocity model, where the medium velocities of the upper and lower layers were 2000 m/s and 3000 m/s, is presented in Figure 7.

In this work, the fourth trace signal of the modeling section was taken as a research object. The first arrival was picked by the UNet++ at different SNR values by adding the Gaussian noise. Then, after adding -8 dB Gaussian noise, the first arrival of the whole section was picked to verify the feasibility of the UNet++-based picking method. The SNR value was calculated by:

$$\frac{S}{N} = 10 \log_{10} \frac{\sigma_s}{\sigma_n}, \tag{5}$$

where σ_s and σ_n denote the standard deviations of the original signal and the added noise, respectively.

2.6. Noise-Free Simulated Signal Test. The forward modeling signals corresponding to eight sections shown in Figure 7 are presented in Figure 8(a). As shown in Figure 8(a), the first arrival time of the signal was 350 ms. Figures 8(b) and 8(c) showed the intermediate features of the signal shown in Figure 8(a) extracted by C3 and C5 layers of the UNet++, respectively. The local magnification of the signal and its first-arrival picking curve obtained by the UNet++ in the range from 330 ms to 430 ms are presented in Figures 9(a) and 9(b), respectively. The complete prediction results are shown in the dotted box in Figure 9(b).

2.7. Gaussian Noise-Added Signal Test. In order to further verify the UNet++ performance in the first-arrival picking of low-SNR microseismic effective signals, the Gaussian noises of -3 dB, -5 dB, and -8 dB were added to the simulated signal shown in Figure 8(a), respectively. The obtained results are presented in Figure 10, Figure 11, and Figure 12.

The forward modeling simulated signals added with the Gaussian noises of -3 dB, -5 dB, and -8 dB are presented in Figures 13(a), 14(a), and 15(a), respectively. The intermediate features of the signal shown in Figure 13(a) extracted by
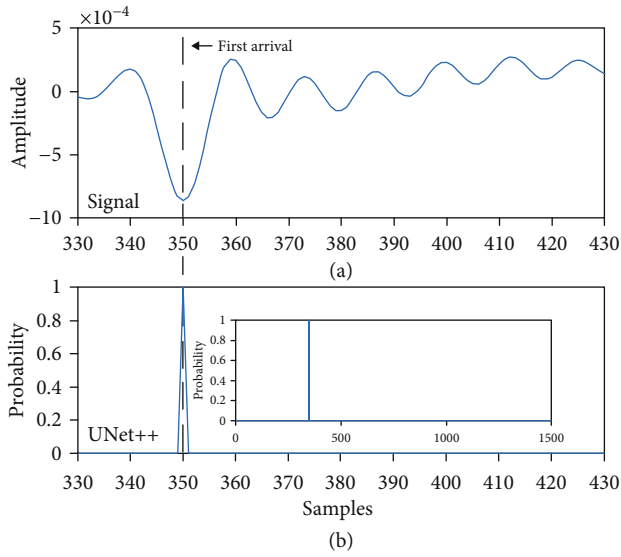
FIGURE 9: First-arrival picking result of the noise-free forward simulated signal. (a) Local amplification of the signal waveform in the range of 330 ms to 430 ms. (b) The picking result in the range from 330 ms to 430 ms obtained by the UNet++.
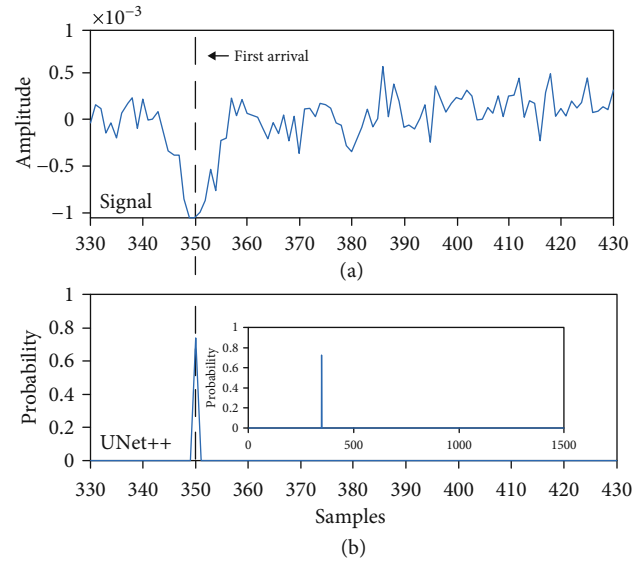

FIGURE 11: First-arrival picking result of the forward modeling signal with -5-dB Gaussian noise added. (a) Local amplification of the signal waveform in the range from 330 ms to 430 ms. (b) The picking result in the range from 330 ms to 430 ms obtained by the UNet++.
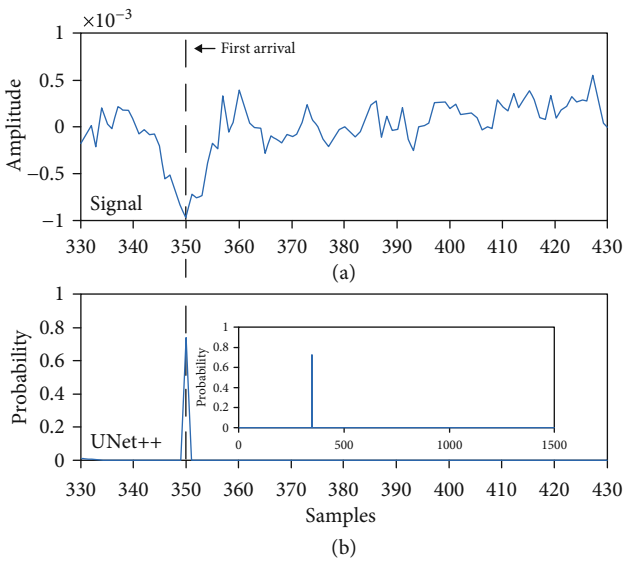

FIGURE 10: First-arrival picking result of the forward modeling signal with -3-dB Gaussian noise added. (a) Local amplification of the signal in the range from 330 ms to 430 ms. (b) The picking result in the range from 330 ms to 430 ms obtained by the UNet++.
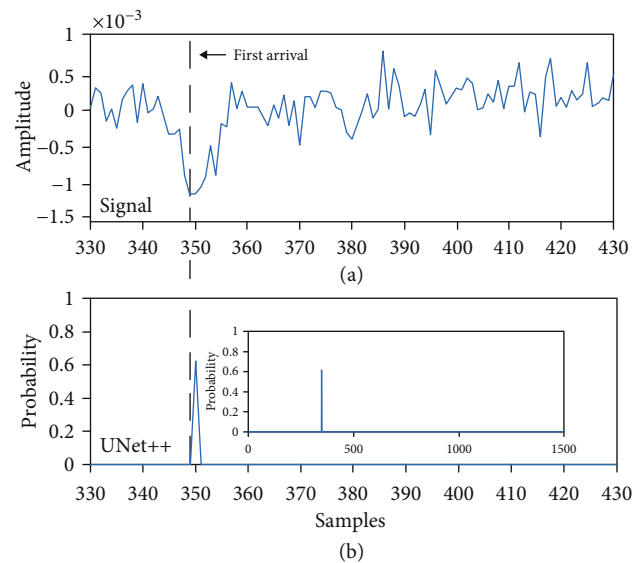

FIGURE 12: First-arrival picking result of the forward modeling signal with -8-dB Gaussian noise added. (a) Local amplification of the signal waveform in the range from 330 ms to 430 ms; (b) the picking result in the range from 330 ms to 430 ms obtained by the UNet++.

C3 and C5 layers of the UNet++ network are presented in Figures 13(b) and 13(c), respectively. The local magnification of the signal and its first-arrival picking curve obtained by the UNet++ in the range from 330 ms to 430 ms are presented in Figures 10(a) and 10(b), respectively. The complete picking result is shown in the dotted box in Figure 10(b).

The intermediate features of the signal shown in Figure 14(a) extracted by C3 and C5 layers of the UNet++ are presented in Figures 14(b) and 14(c), respectively. The local magnification of the signal and its first-arrival picking

curve obtained by the UNet++ in the range from 330 ms to 430 ms are presented in Figures 11(a) and 11(b). The complete picking result is shown in the dotted box in Figure 11(b).

The intermediate features of the signal shown in Figure 15(a) extracted by C3 and C5 layers of the UNet++ are presented in Figures 15(b) and 15(c), respectively. The local magnification of the signal and its first-arrival picking curve obtained by the UNet++ in the range from 330 ms to
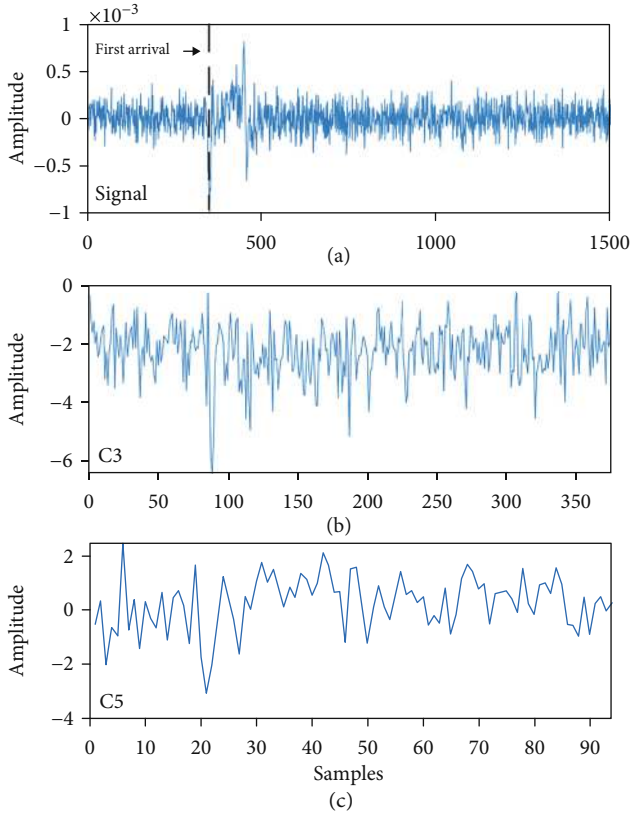
Figure 13: Forward modeling signal with -3-dB Gaussian noise added and its intermediate features extracted by the UNet++. (a) The forward modeling signal with -3-dB Gaussian noise added. (b) Intermediate features of the signal extracted by C3 layer. (c) Intermediate features of the signal extracted by C5 layer.

430 ms are presented in Figures 12(a) and 12(b). The complete picking result is shown in the dotted box in Figure 12(b).

As shown in Figure 9, Figure 10, Figure 11, and Figure 12, as the SNR of the forward modeling simulated signals decreased, the probability of the first-arrival point predicted by the UNet++ declined. This was because the network extracted not only the features of the original signal at the arrival point but also the characteristics of the noise, thus reducing the probability value of the first-arrival point predicted by the network. However, the proposed algorithm could still accurately predict the first-arrival point, which indicates that the first-arrival picking method based on the UNet++ network can pick the first arrival of the effective signal of the low-SNR microseismic signals steadily and accurately.

2.8. Forward Modeling Profile Test. As the distance between the fracture and receiving points increases, the effective signal amplitude gradually decays. In order to evaluate the influence of the signal amplitude on the first-arrival point picking result further, the third trace signal of the profile was taken as a reference trace, and then, -8 dB Gaussian noise was added to the reference trace signal. Finally, the Gaussian noise was added to the reference trace signal to the entire monitoring profile shown in Figure 7 to test the performance
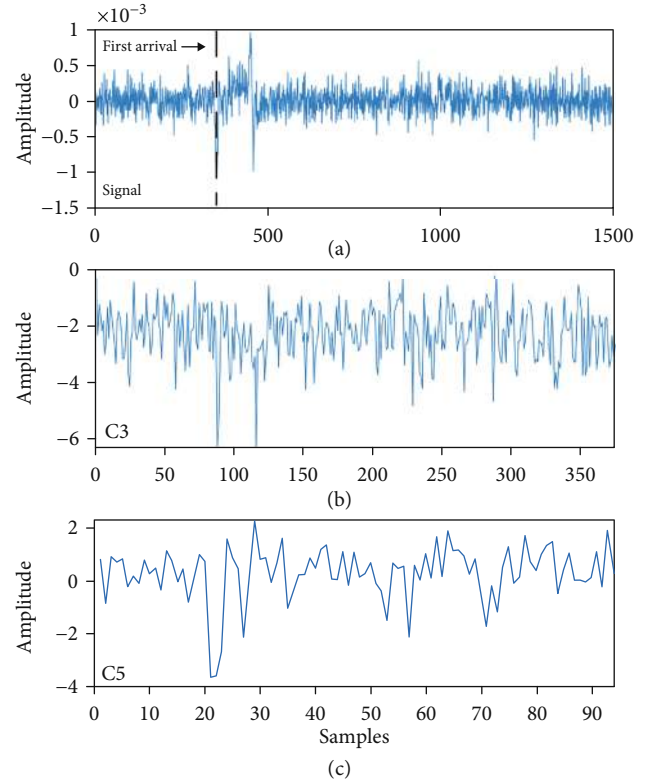

Figure 14: Forward modeling signal with -5-dB Gaussian noise added and its intermediate features extracted by the UNet++. (a) The forward modeling signal with -5-dB Gaussian noise added. (b) Intermediate features of the signal extracted by C3 layer. (c) Intermediate features of the signal extracted by C5 layer.

of the proposed first-arrival picking algorithm. The picking results are shown in Figure 16, and Table 2 shows the specific data of Figure 16(c).

As presented in Figure 16, at the Gaussian noise of -8 dB, the first-arrival picking algorithm based on the UNet++ was more accurate for the synthesized signal profile than the U-Net, and the picking error was only 276 ms. Particularly, the first-arrival picking results of the third eight traces of the monitoring profile were in good agreement with the first-arrival point of the forward modeling simulated signal. This was because the features of the effective signal at the arrival point were more obvious, and the SNR was higher than the first and second signal trace. However, for the first and second signal traces due to the amplitude attenuation of the effective signal, after adding the Gaussian noise, the signal characteristics were unrecognizable, and the SNR was significantly reduced, resulting in a large first-arrival picking error. As can be seen in Figure 16, for low-SNR microseismic signals, the proposed algorithm could efficiently and accurately pick the first arrival of microseismic signals.

2.9. Real Data Examples. In order to verify the feasibility of the proposed algorithm further, the test was conducted on selected microseismic data from Sichuan working area and Shengli oilfield. Also, the U-Net-based arrival picking algorithm and the traditional STA/LTA algorithm, known for its high efficiency, were compared.
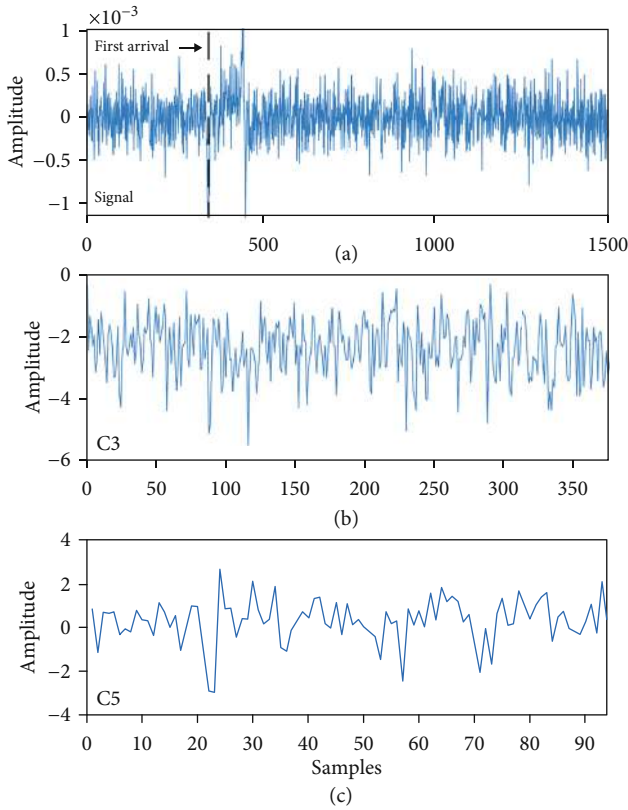
FIGURE 15: Forward modeling signal with -8-dB Gaussian noise added and its intermediate features extracted by the UNet++. (a) The forward modeling signal with -8-dB Gaussian noise added. (b) Intermediate features of the signal extracted by C3 layer. (c) Intermediate features of the signal extracted by C5 layer.

The microseismic records with high SNR obtained by the actual monitoring in a work area of Shengli Oilfield, with seven-level geophones in total, are presented in Figure 17. The length of each signal was 4096 ms, and the sampling interval was 1 ms. The arrival point in the microseismic monitoring record was about 3500–4000 ms. The first trace signal of the actual microseismic signal and the intermediate features extracted by C3 and C5 layers of the UNet++ are presented in Figure 18. The arrival times of the signal shown in Figure 18(a) picked by UNet++, U-Net, and STA/LTA algorithms are shown in Figure 19.

As shown in Figure 19, the picking result obtained by the U-Net and UNet++ for the microseismic monitoring signal shown in Figure 18(a) were both consistent with the manual picking result, whereas the STA/LTA algorithm had an obvious picking error.

The low-SNR microseismic records obtained from the actual monitoring in a work area of Sichuan Province, with nine-level geophones in total, are presented in Figure 20. The length of each signal was 3200 ms, and the sampling interval was 1 ms. The arrival point in the microseismic monitoring record was at about 500 ms; the results obtained by the manual picking are given in Table 3. The sixth trace signal of the microseismic record profile and the intermediate features extracted by C3 and C5 layers of the UNet++ are
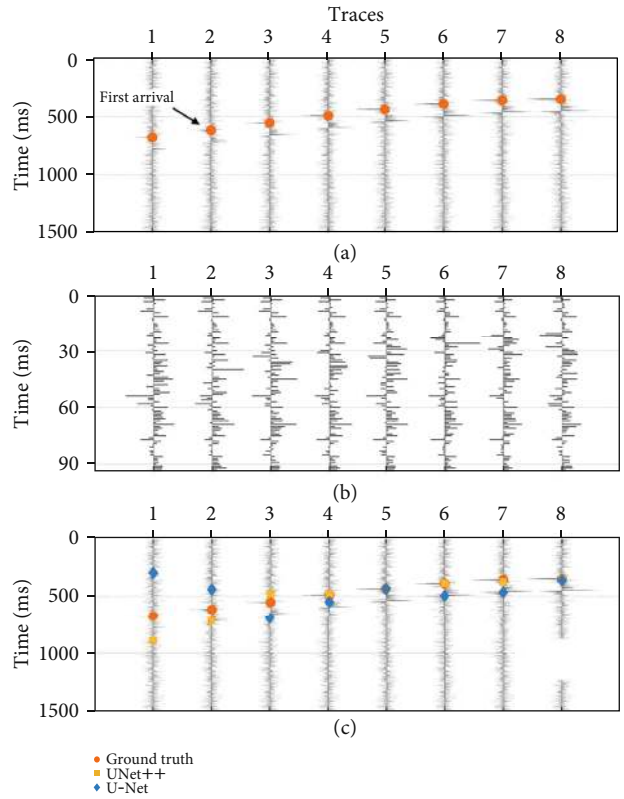

FIGURE 16: First-arrival picking results of the forward modeling profile with -8-dB Gaussian noise added. (a) The noisy profile formed by adding the Gaussian noise with the SNR of -8-dB to the profile shown in Figure 6. (b) The noisy profile intermediate features extracted by C5 layer of the UNet++. (c) First-arrival prediction results obtained by the UNet++ and the U-Net.

TABLE 2: Result comparison of UNet++ and U-Net methods with the ground truth.

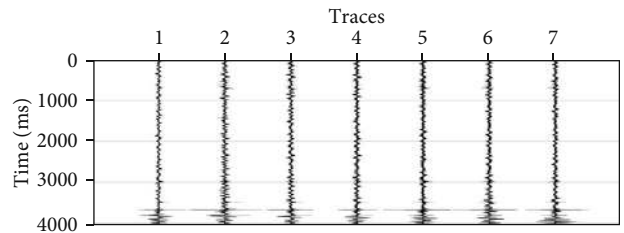| Method	1	2	3	4	5	6	7	8
Ground truth	678	617	554	493	438	392	360	350
UNet++	891	724	552	490	436	392	361	351
U-Net	301	443	697	552	437	498	468	367

FIGURE 17: Actual high-SNR microseismic record profile of a working area in Shengli Oilfield.

presented in Figure 21. Comparison of the first-arrival picking results of the signal shown in Figure 21(a) obtained by the UNet++, U-Net, and STA/LTA algorithms are presented in Figure 22.
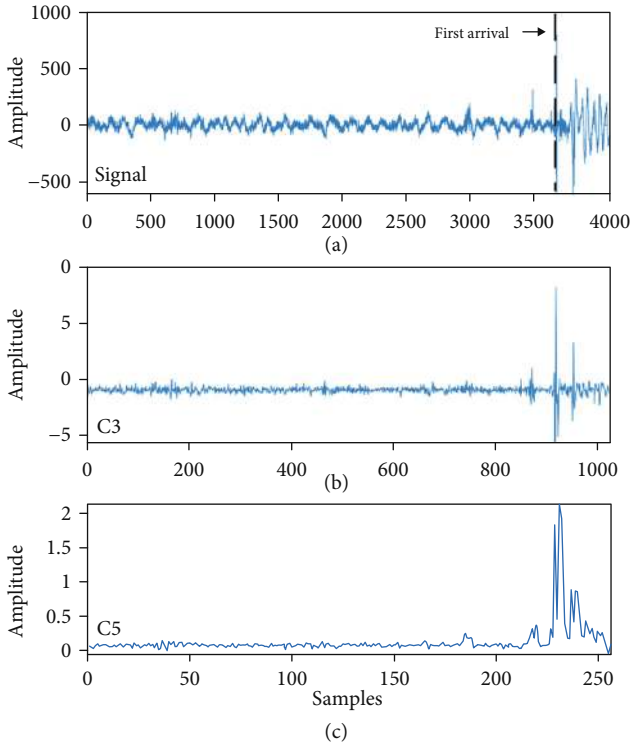
FIGURE 18: The first trace signal of the actual microseismic record profile shown in Figure 17 and its intermediate features extracted by the UNet++. (a) The first trace signal of the actual microseismic record profile shown in Figure 17. (b) Intermediate features of the signal extracted by C3 layer. (c) Intermediate features of the signal extracted by C5 layer.

As shown in Figure 22(a), the UNet++-based picking method could pick the arrival for the low-SNR signal; however, there was s picking error of the U-Net-based first-arrival picking method, and the arrival point picked by the U-Net was 1384. Similarly, the STA/LTA algorithm had an obvious picking error.

Table 3 shows the picking time consumption for the record profiles shown in Figures 17 and 20 of the UNet++, U-Net, and STA/LTA algorithm.

According to the comparison experiment of the simulated and actual monitoring signals and the comparison of first-arrival picking time consumption of different algorithms, it can be concluded that the STA/LTA algorithm, which is famous for its high efficiency, can difficultly obtain accurate first-arrival picking result under the condition of low SNR, while the first-arrival picking algorithm based on deep learning, due to its powerful feature capturing capability and better distinguishing of SNR features, can accurately and efficiently pick the first arrival of low-SNR microseismic signals. The picking speed of the proposed method is significantly higher than that of the STA/LTA algorithm, thus improving both the speed and the accuracy of the first-arrival picking.

The UNet++, due to its layer-to-layer dense connection and deep supervision structure, can extract deeper characteristics of signal and noise than the U-Net and distinguish the microseismic signal even in a low-SNR environment. The

FIGURE 19: First-arrival picking result of the signal shown in Figure 18(a). (a) Local amplification of the signal in the range from 3650 ms to 3800 ms. (b) The picking result in the signal band from 3650 ms to 3800 ms obtained by the UNet++. (c) The picking result in the signal band from 3650 ms to 3800 ms obtained by the U-Net. (d) The picking result in the signal band from 3650 ms to 3800 ms obtained by the STA/LTA for the long- and short-time windows of 300 and 100, respectively.
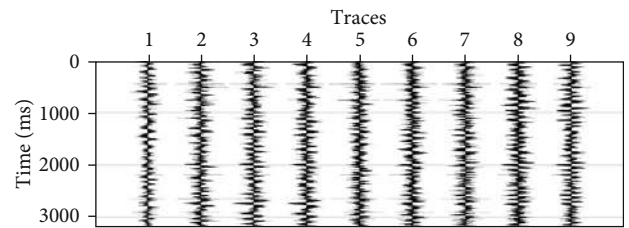
FIGURE 20: Actual low-SNR microseismic record profile of a working area in Sichuan Province.
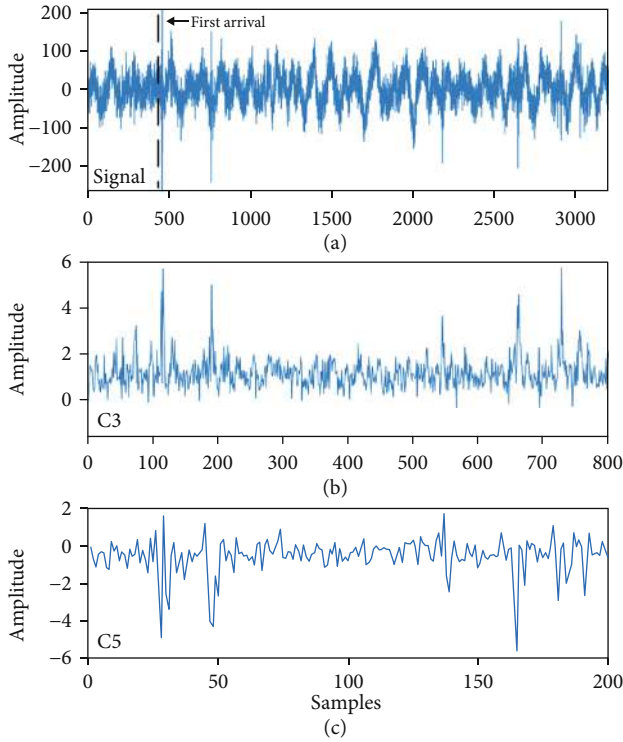
Figure 21: The sixth trace signal of the actual microseismic record profile shown in Figure 20 and its intermediate features extracted by the UNet++. (a) The sixth trace signal of the actual microseismic record profile shown in Figure 20. (b) Intermediate features of the signal extracted by C3 layer. (c) Intermediate features of the signal extracted by C5 layer.

excellent generalization ability further expands its application prospect in the first-arrival picking of microseismic signals. Consequently, the proposed first-arrival picking algorithm based on the UNet++ can pick the arrivals of microseismic signals more accurately and efficiently.

3. Discussion

Although the proposed method can achieve good results, there is still room for improvement.

Monitoring data of different work areas differ in monitoring methods, geological conditions, fracturing methods, etc. Thus, labeling of the data of a new survey area can greatly reduce the application efficiency of the algorithm, causing it does not meet the requirements of real-time processing of microseismic monitoring. However, semisupervised learning uses the network to extract the features of labeled data from small samples automatically, thus realizing automatic labeling of large-scale unlabeled data, which can greatly improve the application efficiency of the proposed algorithm [45–47].

Compared to supervised learning, transfer learning continues to learn the target domain data on the basis of initialization using the pretraining network parameters, reducing the training data scale, and greatly decreasing the computational cost and time consumption of network training [48]. Therefore, in order to realize the processing of microseismic
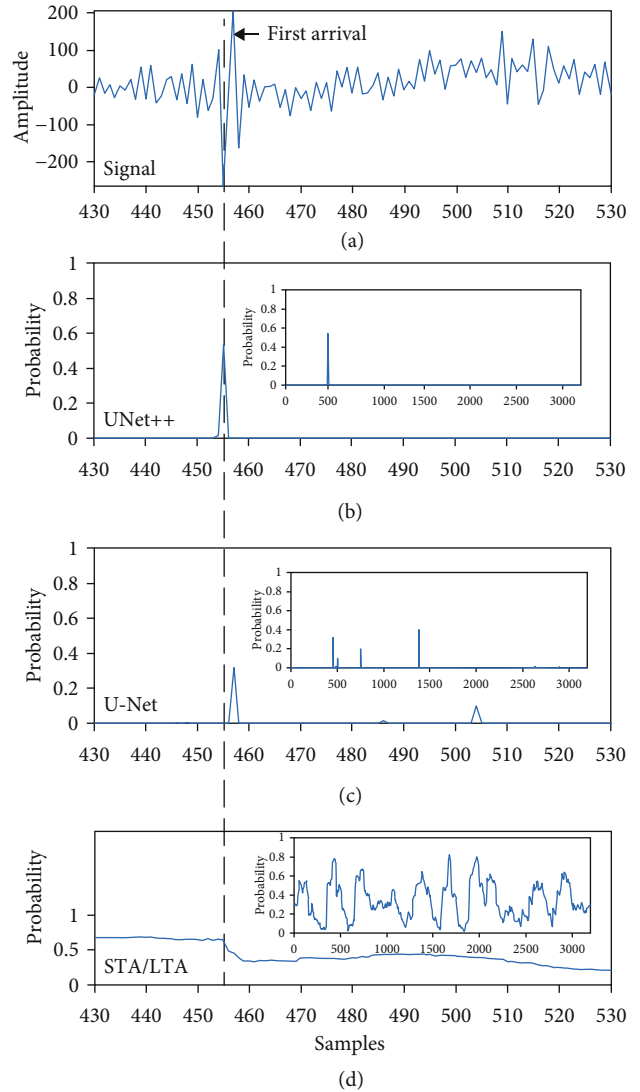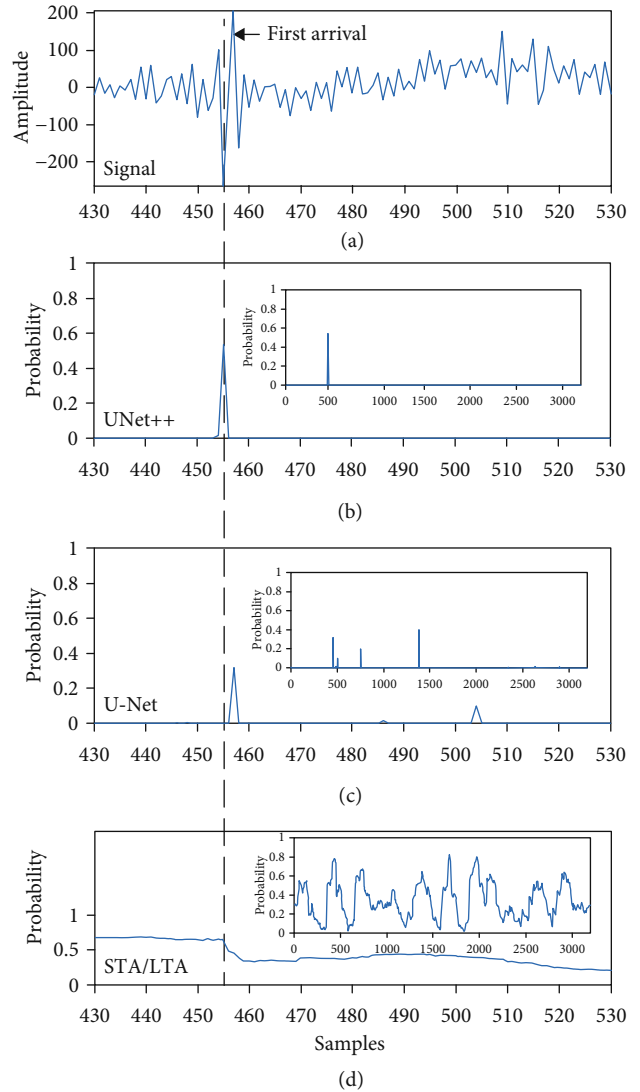

Figure 22: First-arrival picking result of the signal shown in Figure 21(a). (a) Local amplification of the signal in the range from 430 ms to 530 ms; (b) The picking result in the signal band from 430 ms to 530 ms obtained by the UNet++. (c) The picking result in the signal band from 430 ms to 530 ms obtained by the U-Net. (d) The picking result obtained by STA/LTA in the signal band from 430 ms to 530 ms, where the long- and short-time windows were 300 and 100, respectively.

Table 3: Picking time spent comparison of UNet++, U-Net, and STA/LTA.

Method	Average time consumption of signals of different lengths	
	3600 ms	4096 ms
STA/LTA	150.1	220.5
UNet++	**10.5**	**10.7**
U-Net	18.8	19.3

monitoring data in different work areas more efficiently and quickly, the follow-up research will combine the ideas of semisupervised learning and transfer learning to improve

the speed of the proposed first-arrival picking algorithm further.

Sample diversity is one of the important factors affecting the prediction performance of the network. Using an appropriate number of samples can further improve the prediction accuracy of the network. Recently, many sample enhancement methods have been proposed, such as Unsupervised Data Augmentation (UDA) [49] and Generative Adversarial Networks (GAN) [50]. Besides, adversarial training can reduce the error rate on the original independent and identically distributed test set and enhance the fault tolerance of the network by the network training with adversarial training set samples [51, 52]. Therefore, the follow-up research will combine sample enhancement and adversarial training to realize high-precision first-arrival picking of microseismic signals under small sample conditions in order to improve further the accuracy of the proposed first-arrival picking method.

Hyperparameters have a significant impact on the model performance, algorithm running time, and storage cost of the deep neural network. Therefore, automatic configuration and optimization of hyperparameters are very important. Ghahramani has pointed out that Bayesian optimization is one of the most advanced and promising technologies in the artificial intelligence field [53]. Therefore, the following-up research will further study the fast Bayesian optimization scheme for a deep neural network [54], optimize the model, and improve its accuracy [55, 56].

4. Conclusions

In this paper, a first-arrival picking method based on UNet++ is proposed to meet the requirements for picking accuracy and efficiency of real-time processing of microseismic signals. In order to test the validity of the proposed algorithm, Gaussian noise with SNR of -1 dB, -5 dB, and -8 dB was added to the forward modeling signal successively, and the proposed algorithm was compared with the STA/LTA algorithm. Finally, the proposed method, the U-Net-based method, and the STA/LTA method were applied to real microseismic monitoring data of the Sichuan basin and Shengli oil field of China verify the feasibility of the UNet++-based picking method. The test on simulated and real data shows that the proposed picking method can pick the first arrival of the effective signal accurately and obtain a reliable result for microseismic monitoring even for noisy signals.

Data Availability

The data and code are available in https://github.com/RufusGuo/UNet-.

Conflicts of Interest

The author declares that there is no conflict of interest regarding the publication of this paper.

References

[1] N. Iqbal, E. Liu, J. H. McClellan, A. Al-Shuhail, S. I. Kaka, and A. Zerguine, "Detection and denoising of microseismic events using time–frequency representation and tensor decomposition," *IEEE Access*, vol. 6, pp. 22993–23006, 2018.

[2] S. C. Maxwell, J. Rutledge, R. Jones, and M. Fehler, "Petroleum reservoir characterization using downhole microseismic monitoring," *Geophysics*, vol. 75, no. 5, pp. 75A129–75A137, 2010.

[3] C. Song and T. Alkhalifah, "Microseismic event estimation based on an efficient wavefield inversion," *IEEE Journal of Selected Topics in Applied Earth Observations and Remote Sensing*, vol. 12, no. 11, pp. 4664–4671, 2019.

[4] G. L. Feng, X. T. Feng, B. R. Chen, and Y. X. Xiao, "A highly accurate method of locating microseismic events associated with rockburst development processes in tunnels," *IEEE Access*, vol. 5, pp. 27722–27731, 2017.

[5] L. Dong, D. Sun, X. Li, and K. Du, "Theoretical and experimental studies of localization methodology for AE and microseismic sources without pre-measured wave velocity in mines," *IEEE Access*, vol. 5, pp. 16818–16828, 2017.

[6] P. M. Duncan and L. Eisner, "Reservoir characterization using surface microseismic monitoring," *Geophysics*, vol. 75, no. 5, pp. 75A139–75A146, 2010.

[7] L. Eisner, P. M. Duncan, W. M. Heigl, and W. R. Keller, "Uncertainties in passive seismic monitoring," *The Leading Edge*, vol. 28, no. 6, pp. 648–655, 2012.

[8] R. Allen, "Automatic earthquake recognition and timing from single trace," *Bulletin of the Seismological Society of America*, vol. 68, no. 5, pp. 1521–1532, 1978.

[9] C. Suhendi, M. R. P. Sudibyo, I. F. Erlangga, and A. P. Arbad, "Automatic event identification from tectonic earthquakes with modified Akaike Information Criterion (mAIC)," in *IOP Conference Series: Earth and Environmental Science, Institut Teknologi Sumatera Campus*, vol. 258, Lampung Selatan, Indonesia, 2019, no. 1, article 012037.

[10] M. Senkaya and H. Karsli, "A semi-automatic approach to identify first arrival time: the cross-correlation technique," *Earth Sciences Research Journal*, vol. 18, no. 2, pp. 107–113, 2014.

[11] G. Sheng, X. Tang, K. Xie, and J. Xiong, "Hydraulic fracturing microseismic first arrival picking method based on non-subsampled shearlet transform and higher-order-statistics," *Journal of Seismic Exploration*, vol. 28, no. 6, pp. 593–618, 2019.

[12] N. Shimoda, A. Reshetnikov, and S. A. Shapiro, "Arrival time picking on common receiver gather for borehole array datas," in *SEG Technical Program Expanded Abstracts 2015*, pp. 2655–2659, Society of Exploration Geophysicists, 2015.

[13] Y. Tan and C. He, "Improved methods for detection and arrival picking of microseismic events with low signal-to-noise ratios," *Geophysics*, vol. 81, no. 2, pp. KS133–KS151, 2016.

[14] V. Karastathis, T. Aspiotis, A. Tselentis, and N. Russill, "Automatic S-wave picking based on time-frequency analysis for passive seismic applications," in *SEG Technical Program Expanded Abstracts 2016*, pp. 2760–2764, Society of Exploration Geophysicists, 2016.

[15] F. Massin and A. Malcolm, "A better automatic body-wave picker with broad applicability," in *SEG Technical Program Expanded Abstracts 2016*, pp. 2617–2621, Society of Exploration Geophysicists, 2016.

[16] J. Akram and D. W. Eaton, "A review and appraisal of arrival-time picking methods for downhole microseismic data," *Geophysics*, vol. 81, no. 2, pp. KS67–KS87, 2016.

[17] D. Kim, J. Byun, M. Lee, J. Choi, and M. Kim, "Fast first arrival picking algorithm for noisy microseismic data," *Exploration Geophysics*, vol. 48, no. 2, pp. 131–136, 2016.

[18] Z. Yu, C. He, G. Hou, and Y. Tan, "Arrival Picking and Refinement for Microseismic Events Based on Waveform Cross-Correlation," in *International Geophysical Conference*, pp. 1354–1357, Beijing, China, 2018.

[19] A. G. Raj, M. C. JH, N. Iqbal, A. A. Al-Shuhail, and S. I. Kaka, "Automatic microseismic event detection using constant false alarm rate processing in time-frequency domain," in *SEG Technical Program Expanded Abstracts 2018*, pp. 2912–2916, Society of Exploration Geophysicists, 2018.

[20] S. Qu, Z. Guan, E. Verschuur, and Y. Chen, "Automatic high-resolution microseismic event detection via supervised machine learning," *Geophysical Journal International*, vol. 222, no. 3, pp. 1881–1895, 2020.

[21] H. Wu, B. Zhang, F. Li, and N. Liu, "Semi-automatic first arrival picking of micro-seismic events by using pixel-wise convolutional image segmentation method," *Geophysics*, vol. 84, no. 3, pp. 1–70, 2019.

[22] L. Gao, Z.-Y. Jiang, and F. Min, "First-arrival travel times picking through sliding windows and fuzzy c-means," *Mathematics*, vol. 7, no. 3, p. 221, 2019.

[23] S. Li, B. Liu, Y. Ren et al., "Deep learning inversion of seismic data," 2020, https://arxiv.org/abs/1901.07733.

[24] G. Zhang, Z. Wang, and Y. Chen, "Deep learning for seismic lithology prediction," *Geophysical Journal International*, vol. 215, no. 2, pp. 1368–1387, 2018.

[25] M. Zhang, Y. Liu, and Y. Chen, "Unsupervised seismic random noise attenuation based on deep convolutional neural network," *IEEE Access*, vol. 7, pp. 179810–179822, 2019.

[26] B. Liu, S. Yang, Y. Ren, X. Xu, P. Jiang, and Y. Chen, "Deep-learning seismic full-waveform inversion for realistic structural models," *Geophysics*, vol. 86, no. 1, pp. R31–R44, 2021.

[27] A. Krizhevsky, I. Sutskever, and G. Hinton, "ImageNet classification with deep convolutional neural networks," *Advances in neural information processing systems*, vol. 25, no. 2, pp. 1097–1105, 2012.

[28] K. Zhang, Y. Guo, X. Wang, J. Yuan, and Q. Ding, "Multiple feature reweight DenseNet for image classification," *IEEE Access*, vol. 7, pp. 9872–9880, 2019.

[29] L. Han, X. Li, and Y. Dong, "Convolutional edge constraint-based U-net for salient object detection," *IEEE Access*, vol. 7, pp. 48890–48900, 2019.

[30] Z. Qu, W. Wang, C. Hou, and C. Hou, "Radar signal intra-pulse modulation recognition based on convolutional denoising autoencoder and deep convolutional neural network," *IEEE Access*, vol. 7, pp. 112339–112347, 2019.

[31] X. Yang, H. Sun, X. Sun, M. Yan, Z. Guo, and K. Fu, "Position detection and direction prediction for arbitrary-oriented ships via multitask rotation region convolutional neural network," *IEEE Access*, vol. 6, pp. 50839–50849, 2018.

[32] Z. Xu, T. Wang, S. Xu et al., "Active source seismic identification and automatic picking of the P-wave first arrival using a convolutional neural network," *Earthquake Research in China*, vol. 33, no. 2, pp. 288–304, 2019.

[33] Y. Chen, G. Zhang, M. Bai, S. Zu, Z. Guan, and M. Zhang, "Automatic waveform classification and arrival picking based on convolutional neural network," *Earth and Space Science*, vol. 6, no. 7, pp. 1244–1261, 2019.

[34] Y. Chen, "Automatic microseismic event picking via unsupervised machine learning," *Geophysical Journal International*, vol. 222, pp. 1750–1764, 2020.

[35] Y. Chen, "Fast waveform detection for microseismic imaging using unsupervised machine learning," *Geophysical Journal International*, vol. 215, no. 2, pp. 1185–1199, 2018.

[36] G. Zhang, C. Lin, and Y. Chen, "Convolutional neural networks for microseismic waveform classification and arrival picking," *Geophysics*, vol. 85, no. 4, pp. WA227–WA240, 2020.

[37] O. M. Saad and Y. Chen, "Automatic waveform-based source-location imaging using deep learning extracted microseismic signals," *Geophysics*, vol. 85, no. 6, pp. KS171–KS183, 2020.

[38] O. M. Saad and Y. Chen, "Earthquake detection and P-wave arrival time picking using capsule neural network," *IEEE Transactions on Geoscience and Remote Sensing*, vol. 58, pp. 1–10, 2021.

[39] D. Peng, Y. Zhang, and H. Guan, "End-to-end change detection for high resolution satellite images using improved UNet++," *Remote Sensing*, vol. 11, no. 11, p. 1382, 2019.

[40] Y. Chen, W. Xu, J. Zuo, and K. Yang, "The fire recognition algorithm using dynamic feature fusion and IV-SVM classifier," *Cluster Computing*, vol. 22, pp. 7665–7675, 2018.

[41] Z. Zhou, M. M. R. Siddiquee, N. Tajbakhsh, and J. Liang, "UNet++: redesigning skip connections to exploit multiscale features in image segmentation," *IEEE transactions on medical imaging*, vol. 39, no. 6, pp. 1856–1867, 2019.

[42] Z. Chu, T. Tian, R. Feng, and L. Wang, "Sea-Land Segmentation with Res-UNet and Fully Connected CRF," in *IGARSS 2019-2019 IEEE International Geoscience and Remote Sensing Symposium*, pp. 3840–3843, IEEE, Yokohama, Japan, 2019.

[43] H. Chen, R. Guo, J. Liu, Y. Wang, and R. Lin, "Magnetotelluric Data Denoising with Recurrent Neural Network," in *SEG 2019 Workshop: Mathematical Geophysics: Traditional vs Learning*, pp. 5–7, Beijing, China, Society of Exploration Geophysicists, 2020.

[44] Z. Zhou, M. M. Siddiquee, N. Tajbakhsh, and J. Liang, "UNet++: A Nested U-Net Architecture for Medical Image Segmentation," in *Deep learning in medical image analysis and multimodal learning for clinical decision support*, pp. 3–11, Springer, Cham, 2018.

[45] S. Laine and T. Aila, "Temporal Ensembling for Semi-Supervised Learning," 2017, https://arxiv.org/abs/1610.02242.

[46] W. Li, L. Duan, D. Xu, and I. W. Tsang, "Learning with augmented features for supervised and semi-supervised heterogeneous domain adaptation," *IEEE Transactions on Pattern Analysis and Machine Intelligence*, vol. 36, no. 6, pp. 1134–1148, 2014.

[47] H. Pan and Z. Kang, "Robust Graph Learning for Semi-Supervised Classification," in *2018 10th International Conference on Intelligent Human-Machine Systems and Cybernetics (IHMSC)*, pp. 265–268, Hangzhou, China, 2018.

[48] X. Li, Y. Grandvalet, and F. Davoine, "Explicit Inductive Bias for Transfer Learning with Convolutional Networks," in *International Conference on Machine Learning*, Stockholmsmässan, Stockholm Sweden, 2018.

[49] Q. Xie, Z. Dai, E. Hovy, M. Luong, and Q. V. Le, "Unsupervised Data Augmentation for Consistency Training," 2019, https://arxiv.org/abs/1904.12848.

[50] C. Chang, T. Chen, and P. Chung, "Semi-supervised Learning Using Generative Adversarial Networks," in *2018 IEEE Symposium Series on Computational Intelligence (SSCI)*, pp. 892–896, Bangalore, India, 2018.

[51] I. J. Goodfellow, J. Shlens, and C. Szegedy, "Explaining and Harnessing Adversarial Examples," 2015, https://arxiv.org/abs/1412.6572.

[52] T. Miyato, S. Maeda, M. Koyama, and S. Ishii, "Virtual adversarial training: a regularization method for supervised and semi-supervised learning," *IEEE Transactions on Pattern Analysis and Machine Intelligence*, vol. 41, no. 8, pp. 1979–1993, 2019.

[53] G. Zoubin, "Probabilistic machine learning and artificial intelligence," *Nature*, vol. 521, no. 7553, pp. 452–459, 2018.

[54] K. Aaron, "Fast Bayesian Optimization of Machine Learning Hyperparameters on Large Datasets," in *Artificial Intelligence and Statistics*, pp. 528–536, PMLR, Fort Lauderdale, Florida, USA, 2017.

[55] A. Karbalayghareh, X. Qian, and E. R. Dougherty, "Optimal Bayesian transfer learning," *IEEE Transactions on Signal Processing*, vol. 66, no. 14, pp. 3724–3739, 2018.

[56] A. H. Liu, Z. Cheng, and J. Jiang, "Bayesian Network Learning for Classification via Transfer Method," in *2019 IEEE 31st International Conference on Tools with Artificial Intelligence (ICTAI)*, pp. 1102–1109, Portland, OR, USA, 2019.